Published in final edited form as:

Exp Eye Res. 2022 May ; 218: 109028. doi:10.1016/j.exer.2022.109028.

Conditional knockout of hephaestin in the neural retina disrupts retinal iron homeostasis

Kevin R. Zhang[a,*], **Bailey Baumann**[a,*], **Ying Song**[a], **Jacob Sterling**[a], **Elizabeth A. Erler**[a], **Samyuktha Guttha**[a], **Zbynek Kozmik**[b], **Joshua L. Dunaief**[§,a]

[a]F.M. Kirby Center for Molecular Ophthalmology, Scheie Eye Institute, Perelman School of Medicine at the University of Pennsylvania, 305 Stellar-Chance Laboratory, 422 Curie Blvd., Philadelphia, PA 19104, USA.

[b]Institute of Molecular Genetics, Academy of Sciences of the Czech Republic, Prague, ASCR, v. v. i. Vídeňská 1083, 142 20 Prague 4, Czech Republic

Abstract

Iron accumulation has been implicated in degenerative retinal diseases. It can catalyze the production of damaging reactive oxygen species. Previous work has demonstrated iron accumulation in multiple retinal diseases, including age-related macular degeneration and diabetic retinopathy. In mice, systemic knockout of the ferroxidases ceruloplasmin (*Cp*) and hephaestin (*Heph*), which oxidize iron, results in retinal iron accumulation and iron-induced degeneration. To determine the role of Heph in the retina, we generated a neural retina-specific *Heph* knockout on a background of systemic *Cp* knockout. This resulted in elevated neural retina iron. Conversely, retinal ganglion cells had elevated transferrin receptor and decreased ferritin, suggesting diminished iron levels. The retinal degeneration observed in systemic $Cp^{-/-}$, $Heph^{-/-}$ mice did not occur. These findings indicate that Heph has a local role in regulating neural retina iron homeostasis, but also suggest that preserved Heph function in either the RPE or systemically mitigates the degeneration phenotype observed in the systemic $Cp^{-/-}$, $Heph^{-/-}$ mice.

Keywords

retina; iron; ferrous; ceruloplasmin; hephaestin; age-related macular degeneration

1. Introduction

Iron is essential for numerous biochemical processes. However, ferrous iron (Fe^{2+}) can catalyze the production of hydroxyl radical, the most damaging free radical (Beard, 2001).

[§]Correspondence to: Joshua L. Dunaief, jdunaief@upenn.edu, F.M. Kirby Center for Molecular Ophthalmology, Scheie Eye Institute, Perelman School of Medicine at the University of Pennsylvania, 305 Stellar-Chance Laboratory, 422 Curie Blvd., Philadelphia, PA 19104, USA. Tel: +1 215 898 5235.

[*]Co-first authors

Because of its high oxygen tension and high concentration of polyunsaturated fatty acids in the photoreceptors, the retina is especially vulnerable to damage by free radicals. Retinal iron accumulation causes degeneration in ocular siderosis (Casini et al., 2020) and may contribute to other retinal diseases, including age-related macular degeneration (AMD) (Hahn et al., 2003), the leading cause of irreversible blindness in the elderly in developed nations (Harvey, 2003), and Stargardt's Disease (Zhao et al., 2021). Understanding the mechanism of retinal iron regulation will enhance understanding of the pathogenesis of retinal diseases involving dysregulated iron metabolism.

Cellular iron transport is regulated by several proteins controlling iron import and export. There are two cellular iron import pathways, non-transferrin bound (NTBI) and transferrin-bound (TBI) iron import, while there is only one mechanism of cellular iron export, which is facilitated by the only known mammalian iron exporter, ferroportin (Fpn) (Donovan et al., 2005). Ceruloplasmin (Cp) and hephaestin (Heph) are homologous ferroxidase proteins that facilitate ferroportin-mediated iron export (Domenico et al., 2007; Syed et al., 2002). Heph and Cp oxidize ferrous (Fe^{2+}) to ferric (Fe^{3+}) iron. Once oxidized to its ferric form, iron can bind transferrin, the extracellular iron transport protein. As Heph and Cp have redundant functions, tissues often express only one of the ferroxidases. However, both *Heph* and *Cp* are expressed within the neural retina and retinal pigment epithelium (RPE) (Hahn et al., 2004).

The importance of the ferroxidases for retinal health is demonstrated by the phenotype of patients with aceruloplasminemia, a rare autosomal recessive disease. These patients have loss of function mutations in the *Cp* gene, resulting in retinal iron accumulation and associated RPE pigmentation changes, and, in one patient, early onset maculopathy resembling AMD (Dunaief et al., 2005; Wolkow et al., 2011). Similarly, mice with systemic KO of both ceruloplasmin and hephaestin ($Cp^{-/-}$, $Heph^{-/-}$ mice) demonstrate retinal iron accumulation and consequent retinal degeneration, with features that resemble both the molecular and histologic features of AMD (Hadziahmetovic et al., 2008). Curiously, mice with knockout of only *Cp* do not have retinal degeneration and only a very mild increase in retinal iron (Hahn et al., 2004). While the reason for this species difference is not known, in theory, it could result from slow, gradual iron accumulation during the longer lifespan of humans, or from higher levels of *Heph* compensating in mouse retinas. Systemic iron chelation treatment ameliorates the retinal degeneration seen in the systemic $Cp^{-/-}$, $Heph^{-/-}$ mice (Hadziahmetovic et al., 2011b), confirming that iron toxicity is the mechanism of retinal degeneration.

However, the local role of Heph in the neurosensory retina is unclear. In AMD and aceruloplasminemia, as well as the systemic $Cp^{-/-}$, $Heph^{-/-}$ mouse model, the RPE has the most pronounced iron accumulation. Our previous work demonstrated that RPE-specific loss of *Heph* on a systemic $Cp^{-/-}$ background leads to iron accumulation primarily in the RPE (Wolkow et al., 2012). Therefore, loss of RPE ferroxidases alone does not explain the neural retina iron accumulation seen in the systemic $Cp^{-/-}$, $Heph^{-/-}$ mice, indicating that either ferroxidase expression in the neural retina, or systemic changes in the $Cp^{-/-}$, $Heph^{-/-}$ mice, such as increased ferrous iron in the blood, are responsible for iron accumulation in the neural retina. It is also unknown whether iron accumulation within the neural retina

specifically is sufficient to cause the retinal degeneration seen in the systemic *Cp*$^{-/-}$, *Heph*$^{-/-}$ mice.

To answer these questions, we developed a neural retina-specific *Heph* KO model on a *Cp* null genetic background, using the mRx-Cre mouse line (Klimova et al., 2013) and a *Heph*-flox line that we developed previously (Wolkow et al., 2012). We found that loss of Heph function in the neural retina caused iron accumulation within most cells of the neural retina, including amacrine and bipolar cells. However, neural retina specific *Heph* KO did not cause retinal degeneration in the neural retina or RPE. These data suggest ferroxidase function in the neural retina affects retinal iron homeostasis, but ferroxidase loss from the neural retina does not fully explain the more substantial iron accumulation and retinal degeneration observed in mice with systemic knockout of both *Cp* and *Heph*.

2. Materials and Methods

2.1 Generation of mRx-Cre experimental mice

Cp$^{-/-}$, *Heph*$^{flox/flox}$ mice were generated as previously described (Harris et al., 1999; Wolkow et al., 2012). To generate the mRx-Cre experimental mice, *Cp*$^{-/-}$, *Heph*$^{flox/flox}$ mice were crossed to mRx-Cre+ mice (Klimova et al., 2013). Mice were on a C57BL/6J background, confirmed negative for *rd1* and *rd8*. Cre activity within the neural retina was confirmed by crossing mRx-Cre+ mice with a mouse line containing a red/green reporter (Fig 1; ROSA$^{mT/mG}$, Jackson Labs stock 7676). mRx-Cre experimental mice had the genotype mRx-Cre+, *Cp*$^{-/-}$, *Heph*$^{flox/flox}$. Unless otherwise indicated, control mice were mRx-Cre+, *Cp*$^{-/-}$, *Heph*$^{+/+}$.

2.2 Fixation of eyes and preparation of eyecups

mRx-Cre experimental and control mice were aged between 6 and 12 months and euthanized. Experimental procedures were performed in accordance with the Association for Research in Vision and Ophthalmology (ARVO) statement for the use of animals in ophthalmology and vision research. All protocols were approved by the University of Pennsylvania animal care review board. Eye fixation and eyecup preparation were performed as previously described (Shu et al., 2019).

2.3 Immunofluorescence

Immunofluorescence was performed on 10 μm thick cryosections as described previously (Hadziahmetovic et al., 2011a). The following antibodies were used: rabbit anti-light ferritin (E17) (1:2500; M. Poli and P. Arosio, University of Brescia, Italy), rat anti-transferrin receptor (1:200; Serotec, Langford Lane, Kidlington, OX5 1GE, UK), and goat anti-Brn-3a (1:200; Santa Cruz, Santa Cruz, CA, USA). Control sections were treated identically but with the primary antibody omitted. Sections were imaged by fluorescence microscopy with identical exposure parameters across genotypes using Nikon Elements software (Melville, NY, USA). Pixel density analysis of the L-ferritin and transferrin receptor immunolabeling were completed using FIJI software (Schindelin et al., 2012). The percentage of RGC cells that were co-labeled with TfR and Brn3a was determined by a masked observer who

counted the number of Brn3a+ cells per section and determined the percentage of Brn3a+ cells that were TfR+.

2.4 Dissection of murine RPE and retinas for RT-PCR

Murine RPE and retinas were dissected and processed for RT-PCR as previously described (Hadziahmetovic et al., 2011c). Briefly, mice were euthanized and the eyes were immediately enucleated. The retina was dissected away from the RPE, flash-frozen, and stored at −80 °C. RPE was mechanically and enzymatically isolated using dispase and hyaluronidase.

2.5 Quantitative Real-Time Polymerase Chain Reaction (qPCR)

RNA was isolated according to the manufacturer's protocol (RNeasy Kit; Qiagen, Valencia, CA, USA). cDNA was synthesized using reverse transcription reagents (TaqMan; Applied Biosystems, Darmstadt, Germany) according to the manufacturer's protocol. Gene expression of *Tfrc*, *Heph*, and *Hamp* were analyzed using quantitative real-time PCR as previously described (Hadziahmetovic et al., 2011a). Gene expression assays (TaqMan; Applied Biosystems, Foster City, CA) were used for PCR analysis, with GAPDH serving as the internal control. RT-PCR was performed on a commercial sequence detection system (ABI Prism 7500; Applied Biosystems, Darmstadt, Germany), and all reactions were performed in technical triplicates (N=3–8 mice per genotype). The following probes were used: *Tfrc* (Mm00441941), *Hamp* (Mm00519025), and custom probe HEPHEX4 that spans *Heph* exon4. The sequences for primers were as follows: forward, 5′-AGGAATACAGTGATGGCACATACAC-3′; reverse, 5′-GCCTGTAACAGTGGTCCTAGGAA-3′; and probe, 5′-AGGCTTGGCTATTTC-3′ (Applied Biosystems, Carlsbad, CA, USA), as suggested by the manufacturer (Wolkow et al., 2012).

2.6 Retinal Ganglion Cell (RGC) Isolation and Purification

Retinal ganglion cells were isolated using the Miltenyi Adult Brain Dissociation Kit (Miltenyi Biotec, 130-107-677) and MACS cell separation system. Briefly, whole neurosensory retinas were harvested, and retinal tissues were dissociated in manufacturer-provided enzyme mixtures using the gentle MACS dissociator pre-set program: 37C_ABDK_01 (Miltenyi Biotec). Dissociated retinal cell suspensions were filtered using a 70 μm filter (Miltenyi Biotec, 130-098-462) and resuspended in debris removal solution. Retinal cells were resuspended and incubated in red blood cell removal solution for 10 minutes at 4 °C. The resulting cell suspension was then subjected to a selection protocol using MACS magnetic separation LS columns (Miltenyi Biotec, 130-042-401) and the following antigen-coated magnetic microbeads: (1) anti-CD11c (Miltenyi Biotec, 130-108-338), (2) anti-ACSA2 (Miltenyi Biotec, 130-097-678), (3) anti-CD45 (Miltenyi Biotec, 130-052-301), (4) anti-CD15 (Miltenyi Biotec, 130-094-530), and a final positive selection step (5) anti-Thy1 (Miltenyi Biotec, 130-121-278), using the manufacturer's protocol to isolate the final target cell population: CD11c− ACSA2− CD45− CD15− Thy1+. RGC enrichment in the final cell fraction was confirmed using qPCR.

2.7 Quantitative liver iron detection

Livers from experimental and age-matched control mice were frozen on dry ice. Dried tissue was digested at 65 °C overnight in acid digest solution (0.1% trichloroacetic acid and 0.03 M HCl). After digestion, samples were centrifuged, and the 20 μL supernatant was added to 1 mL of chromogen reagent (2.25 M sodium acetate pretreated with Chelex 100 (Bio-Rad, Hercules, CA, USA), 0.01% BPS, and 0.1% thioglycolic acid). Absorbance was read at 535 nm. Iron levels were determined by comparing absorbances of tissue-chromogen samples to serial dilutions of iron standard (Sigma-Aldrich, St Louis, MO).

2.8 Morphologic analysis

Morphologic analysis was performed as previously described (Hadziahmetovic et al., 2011a). Briefly, eyes were enucleated, fixed overnight in 2% paraformaldehyde–2% glutaraldehyde, and embedded in JB-4 plastic (Polysciences, Warrington, PA). 3 μm thick sections were stained with toluidine blue.

2.9 Spectral Domain OCT Imaging

Mice were anesthetized with an intraperitoneal injection of (in mg/kg bodyweight): 80 ketamine (Par Pharmaceutical, Spring Valley, NY, USA), 10 xylazine (Lloyd Inc., Shenandoah, IA), and 2 acepromazine (Boehringer Ingelheim Vetmedica, Inc. St. Joseph, MO, USA). Pupils were dilated with 1% tropicamide. As described previously, artificial tears were used throughout the procedure for corneal protection and maintenance of corneal clarity. Mice were seated in the Bioptigen AIM-RAS holder (Hadziahmetovic et al., 2011b). Spectral domain OCT images were obtained using the Envisu R2200-HR SD-OCT device and corresponding image acquisition software (Bioptigen, Durham, NC, USA). A standard horizontal line scan was used, which was at the level of the optic disc. ONL thicknesses for experimental and control mice eyes were compared at the same location.

2.10 Statistical Analysis

Mean ± SEM was calculated for every group, and statistical analysis was performed using Student's two-group, two-tailed *t*-test. For multiple comparisons, one-way ANOVA with *post hoc* pairwise comparisons using the Tukey method was used. All statistical analyses were performed with GraphPad Prism 5.0 (San Diego, CA, USA).

3. Results

3.1 Validation of *Heph* conditional knockout in neural retina

Hephaestin is expressed within all cells of the neural retina with the exception of microglia (Macosko et al., 2015). To verify the ability of the mRx-Cre line to delete floxed sequences within the neural retina, we crossed mRx-Cre+ mice with a line expressing $ROSA^{mT/mG}$. This line constitutively expresses red tdTomato (mT) fluorescence, but upon Cre recombinase expression, expresses green EGFP (mG) fluorescence instead (Muzumdar et al., 2007). We found EGFP fluorescence in all cell types throughout the neural retina of mRx-Cre+, $ROSA^{mT/mG}$ mice, except for blood vessels (Figure 1A; white arrows point to blood vessels). There was EGFP fluorescence in only a few scattered RPE cells (green

arrows, Figure 1A). In contrast, control mRx-Cre-, ROSA$^{mT/mG}$ retinas had red fluorescence throughout the neural retina and RPE.

To generate the experimental mRx-Cre mice, we crossed mRx-Cre+ mice with *Cp*$^{-/-}$, *Heph*$^{flox/flox}$ mice. *Cp* KO on this line has been validated previously (Harris et al., 1999). Neural retina-specific *Heph* KO in the mRx-Cre experimental mice was verified using qPCR. The *Heph* mRNA level was markedly reduced in the neural retina of mRx-Cre experimental mice compared with controls (Figure 1B). *Heph* KO occurred predominantly in the neural retina, as *Heph* mRNA levels were unchanged in the RPE (Figure 1C). To rule out the possibility that there was an effect on systemic iron levels, liver iron levels of controls (mRx-Cre+, *Cp*$^{-/-}$, *Heph*$^{+/+}$) and experimental (mRx-Cre+, *Cp*$^{-/-}$, *Heph*$^{flox/flox}$) mice were compared using both direct and indirect methods. Liver iron concentration was not changed between the control and experimental mice (Figure 1D). Liver hepcidin (*Hamp*) (Figure 1E) and transferrin receptor (*Tfrc*) (Figure 1F) mRNA levels, which would normally be up and down regulated by an increase in intracellular iron, respectively, were unchanged between the experimental and control mice. Hepcidin negatively regulates the cell membrane expression of ferroportin (Fpn), with *Hamp* mRNA levels increased under conditions of liver iron overload (Rivera et al., 2005). Transferrin receptor allows for iron import into the cell, and mRNA levels are downregulated when cells are iron loaded (Rouault et al., 1990). These data demonstrate that, as expected, neural retina-specific *Heph* KO does not alter systemic iron levels, indicating that any changes in retinal iron levels were the result of the loss of *Heph* in the neural retina rather than changes in systemic iron available to the retina.

3.2 Loss of ferroxidases in the neural retina results in retinal iron accumulation

To determine how retinal iron levels were changed with neural retina ferroxidase loss, we used immunohistochemistry to examine levels of transferrin receptor (TfR) and ferritin-L (FtL) in neural retinas of 6-month mice. Ferritin-L is an iron storage protein, with translation upregulated by elevated intracellular iron. Pixel density quantification was used to measure the FtL and TfR immunolabeling from the outer boundary of the inner plexiform layer (IPL) to the inner limiting membrane, given that FtL is expressed at the highest levels in these retinal layers (Hahn et al., 2004).

There was evidence of neural retinal iron accumulation of the mRx-Cre+, *Cp*$^{-/-}$, *Heph*$^{flox/flox}$ based on increased FtL immunoreactivity in the inner plexiform layer and in amacrine cells located in the innermost layers of the INL (Figure 2A, B) compared to age-matched controls. Systemic *Cp*$^{-/-}$, *Heph*$^{-/-}$ mice displayed an even greater increase in FtL immunoreactivity. Overall inner retina TfR immunoreactivity was not changed between control and mRx-Cre+, *Cp*$^{-/-}$, *Heph*$^{flox/flox}$ mice, although systemic *Cp*$^{-/-}$, *Heph*$^{-/-}$ mice displayed significantly reduced TfR immunoreactivity (Figure 2A, C). In mRx-Cre+, *Cp*$^{-/-}$, *Heph*$^{flox/flox}$ mice, TfR increased in a subset of cells, particularly in the ganglion cell layer (GCL). As expected, there was very little co-localization of FtL and TfR, since levels of these two iron regulated proteins move in opposite directions as intracellular iron levels change.

3.3 Experimental mice have elevated TfR in retinal ganglion cells (RGCs)

Immunofluorescence showed elevated levels of TfR protein in the GCL in experimental mice, with the same cells displaying low ferritin-L labeling (Figure 2). High TfR and low ferritin is a profile suggesting low iron levels in these cells. To test if the TfR+ cells in the GCL were retinal ganglion cells (RGCs) or amacrine cells, we co-labeled retina sections from control and mRx-Cre+, $Cp^{-/-}$, $Heph^{flox/flox}$ 6-month-old mice for TfR and Brn3a, an RGC-specific marker (Figure 3A). Strong signal for TfR was found surrounding RGC nuclei (green arrows, Figure 3A). There was a significantly increased percentage of cells co-labeling for Brn3a and TfR in experimental mice compared to controls (Figure 3B). Furthermore, in isolated RGCs from 8-month-old experimental mice, transferrin receptor (*Tfrc)* mRNA levels were significantly increased relative to age-matched controls (Figure 3C). These results suggest RGC iron depletion.

3.4 No evidence of retinal degeneration in mRx-Cre experimental mice

Systemic loss of ferroxidases in the $Cp^{-/-}$, $Heph^{-/-}$ mice results in neural retinal iron accumulation by 6 months (Hadziahmetovic et al., 2008) and retinal degeneration by 9 months (Hahn et al., 2004). Similarly, loss of RPE ferroxidases leads to mild RPE iron accumulation at 9 months and, at 12 months, some aspects of the RPE degeneration seen in the systemic $Cp^{-/-}$, $Heph^{-/-}$ mice (Wolkow et al., 2012). To determine whether iron accumulation within the neural retina was sufficient to alter retinal morphology in mRx-Cre experimental mice, we preformed several tests on 12-month-old mice, including imaging with *in vivo* retinal photography and optical coherence tomography (OCT), and morphological analysis of plastic sections. Micron III fundus photography (Figure 4A), histological analysis (Figure 4B), and OCT (Figure 4C) all showed no differences between experimental and control mice. There was no decrease in ONL thickness, indicating lack of retinal degeneration (Figure 4D).

4. Discussion

To better understand the mechanisms contributing to retinal iron overload in AMD and other retinal degenerative diseases, we must first understand mechanisms of retinal iron homeostasis. Using an animal model of the autosomal recessive disease aceruloplasminemia, we have previously demonstrated that systemic loss of homologous ferroxidases *Cp* and *Heph* leads to retinal iron overload by 6 months and retinal degeneration by 9 months of age (Hadziahmetovic et al., 2008; Hahn et al., 2004). Cp and Heph must have overlapping functions, as loss of either protein alone does not result in neural retina iron accumulation (Hahn et al., 2004). We have also previously demonstrated that, on a $Cp^{-/-}$ background, deletion of *Heph* in the RPE causes some RPE iron accumulation and degeneration, but not as much as in systemic $Cp^{-/-}$, $Heph^{-/-}$ mice (Wolkow et al., 2012). Herein, we found that neural retina-specific deletion of *Heph* on a $Cp^{-/-}$ background led to iron accumulation in the neural retina, as indicated by increases in FtL in the inner retina, but not as much as in systemic $Cp^{-/-}$, $Heph^{-/-}$ mice and without retinal degeneration. Interestingly, FtL signal was absent in a band-like pattern running in the middle of the inner plexiform layer, which may reflect iron depletion in a subset of amacrine cells. Transferrin receptor levels were not measurably diminished in the mRx-Cre+, $Cp^{-/-}$, $Heph^{flox/flox}$ mice, which

may reflect cellular heterogeneity in iron accumulation. The changes in ferritin levels in mRx-Cre+, $Cp^{-/-}$, $Heph^{flox/flox}$ mice indicate that Heph plays a tissue-autonomous role in iron regulation the neural retina, just as in the RPE.

The mechanism of retinal iron accumulation in mRx-Cre+, $Cp^{-/-}$, $Heph^{flox/flox}$ mice could be due to increased iron import or decreased iron export through the sole cellular iron exporter, ferroportin (Fpn), which is known to cooperate with Cp and Heph to export iron. Recent data show that mRx-Cre+, $Fpn^{flox/flox}$ mice do not have iron accumulation in the neural retina (Liu et al., 2022). Those data suggest that impaired iron export from Fpn is not the sole mechanism of retinal iron accumulation in mRx-Cre+, $Cp^{-/-}$, $Heph^{flox/flox}$ mice. Rather, the lack of neural retina ferroxidases is likely to cause an increase in ferrous iron, especially since the eye contains iron-reducing ascorbate at 1 mM (Pirie, 1965), which is twenty-times greater than serum level (Schleicher et al., 2009). This ferrous iron can be taken up through ferrous iron importers such as Zip8, Zip14, and Dmt1, which are expressed in the retina. While cellular import of ferric iron is regulated through transferrin receptor downregulation, Zip8 and Zip14 are not downregulated by neural retina iron overload (Sterling et al., 2017). Rather, in systemic $Cp^{-/-}$, $Heph^{-/-}$ neural retinas, both Zip8 and Zip14 are upregulated (Sterling et al., 2017). Mechanistically, this Zip8 and Zip14 upregulation may be caused by elevated intracellular labile iron inducing inhibition of their membrane extraction (Sterling et al., 2017; Zhao et al., 2014).

While mRx-Cre+, $Cp^{-/-}$, $Heph^{flox/flox}$ mice have elevated iron levels in their IPL and inner portion of the INL, their RGCs appear to have diminished iron levels evidenced by elevated TfR and low FtL immunoreactivity (Figures 2,3). Based on the above findings, RGCs, as well as a subtype of amacrine cells, may be unable to efficiently import ferrous iron.

Our results indicate that ferroxidases expressed within the neural retina are essential for proper iron homeostasis. However, mRx-Cre+, $Cp^{-/-}$, $Heph^{flox/flox}$ mice have less retinal iron accumulation, and no degeneration, compared to systemic $Cp^{-/-}$, $Heph^{-/-}$ mice. This indicates that preserved hephaestin function in the RPE or systemically partially mitigates neural retina iron accumulation. This non-cell-autonomous Heph activity, together with the absence of retinal iron accumulation in retina-specific *Fpn* KO mice (Liu et al., 2022), suggests that Heph's activity in the neural retina may primarily impact iron uptake rather than cellular iron export. It is of interest that ferrous iron importers are not downregulated by intracellular iron levels, and, paradoxically, can be upregulated (Sterling et al., 2017), which could explain the iron overload seen in many retinal diseases.

Acknowledgements

Funding from NIH/NEI EY015240, the UPenn Vision Science Training Grant (5T32EY007035-37), Research to Prevent Blindness, the F.M. Kirby Foundation, a gift in memory of Lee F. Mauger, MD, and the Paul and Evanina Bell Mackall Foundation Trust.

References

Beard JL, 2001. Iron biology in immune function, muscle metabolism and neuronal functioning. J. Nutr 131. 10.1093/JN/131.2.568S

Casini G, Sartini F, Loiudice P, Benini G, Menchini M, 2020. Ocular siderosis: a misdiagnosed cause of visual loss due to ferrous intraocular foreign bodies—epidemiology, pathogenesis, clinical signs, imaging and available treatment options. Doc. Ophthalmol 2020 1422 142, 133–152. 10.1007/S10633-020-09792-X

De Domenico I, Ward DM, di Patti MCB, Jeong SY, David S, Musci G, Kaplan J, 2007. Ferroxidase activity is required for the stability of cell surface ferroportin in cells expressing GPI-ceruloplasmin. EMBO J 26, 2823. 10.1038/SJ.EMBOJ.7601735 [PubMed: 17541408]

Donovan A, Lima CA, Pinkus JL, Pinkus GS, Zon LI, Robine S, Andrews NC, 2005. The iron exporter ferroportin/Slc40a1 is essential for iron homeostasis. Cell Metab 1, 191–200. 10.1016/J.CMET.2005.01.003 [PubMed: 16054062]

Dunaief J, Richa C, Franks E, Schultze R, Aleman T, Schenck J, Zimmerman E, Brooks D, 2005. Macular Degeneration in a Patient with Aceruloplasminemia, a Disease Associated with Retinal Iron Overload. Ophthalmology 112, 1062–1065. 10.1016/j.ophtha.2004.12.029 [PubMed: 15882908]

Hadziahmetovic M, Dentchev T, Song Y, Haddad N, He X, Hahn P, Pratico D, Wen R, Harris ZL, Lambris JD, Beard J, Dunaief JL, 2008. Ceruloplasmin/hephaestin knockout mice model morphologic and molecular features of AMD. Invest. Ophthalmol. Vis. Sci 49, 2728–2736. 10.1167/IOVS.07-1472 [PubMed: 18326691]

Hadziahmetovic M, Song Y, Ponnuru P, Iacovelli J, Hunter A, Haddad N, Beard J, Connor JR, Vaulont S, Dunaief JL, 2011a. Age-Dependent Retinal Iron Accumulation and Degeneration in Hepcidin Knockout Mice. Invest. Ophthalmol. Vis. Sci 52, 109–118. 10.1167/IOVS.10-6113 [PubMed: 20811044]

Hadziahmetovic M, Song Y, Wolkow N, Iacovelli J, Grieco S, Lee J, Lyubarsky A, Pratico D, Connelly J, Spino M, Harris ZL, Dunaief JL, 2011b. The Oral Iron Chelator Deferiprone Protects against Iron Overload–Induced Retinal Degeneration. Invest. Ophthalmol. Vis. Sci 52, 959–968. 10.1167/IOVS.10-6207 [PubMed: 21051716]

Hadziahmetovic M, Song Y, Wolkow N, Iacovelli J, Kautz L, Roth M-P, Dunaief JL, 2011c. Bmp6 Regulates Retinal Iron Homeostasis and Has Altered Expression in Age-Related Macular Degeneration. Am. J. Pathol 179, 335. 10.1016/J.AJPATH.2011.03.033 [PubMed: 21703414]

Hahn P, Milam AH, Dunaief JL, 2003. Maculas Affected by Age-Related Macular Degeneration Contain Increased Chelatable Iron in the Retinal Pigment Epithelium and Bruch's Membrane. Arch. Ophthalmol 121, 1099. 10.1001/archopht.121.8.1099 [PubMed: 12912686]

Hahn P, Qian Y, Dentchev T, Chen L, Beard J, Harris ZL, Dunaief JL, 2004. Disruption of ceruloplasmin and hephaestin in mice causes retinal iron overload and retinal degeneration with features of age-related macular degeneration. Proc. Natl. Acad. Sci. U. S. A 101, 13850–13855. 10.1073/PNAS.0405146101 [PubMed: 15365174]

Harris ZL, Durley AP, Man TK, Gitlin JD, 1999. Targeted gene disruption reveals an essential role for ceruloplasmin in cellular iron efflux. Proc. Natl. Acad. Sci. U. S. A 96, 10812–10817. 10.1073/PNAS.96.19.10812 [PubMed: 10485908]

Harvey PT, 2003. Common eye diseases of elderly people: identifying and treating causes of vision loss. Gerontology 49, 1–11. 10.1159/000066507 [PubMed: 12457044]

Klimova L, Lachova J, Machon O, Sedlacek R, Kozmik Z, 2013. Generation of mRx-Cre transgenic mouse line for efficient conditional gene deletion in early retinal progenitors. PLoS One 8. 10.1371/JOURNAL.PONE.0063029

Liu Y, Baumann B, Song Y, Zhang K, Sterling JK, Lakhal-Littleton S, Kozmik Z, Su G, Dunaief JL, 2022. Minimal effect of conditional ferroportin KO in the neural retina implicates ferrous iron in retinal iron overload and degeneration. Exp. Eye Res 108988. 10.1016/J.EXER.2022.108988 [PubMed: 35202704]

Macosko EZ, Basu A, Satija R, Nemesh J, Shekhar K, Goldman M, Tirosh I, Bialas AR, Kamitaki N, Martersteck EM, Trombetta JJ, Weitz DA, Sanes JR, Shalek AK, Regev A, McCarroll SA, 2015. Highly Parallel Genome-wide Expression Profiling of Individual Cells Using Nanoliter Droplets. Cell 161, 1202–1214. 10.1016/J.CELL.2015.05.002 [PubMed: 26000488]

Muzumdar MD, Tasic B, Miyamichi K, Li L, Luo L, 2007. A global double-fluorescent Cre reporter mouse. Genesis 45, 593–605. 10.1002/DVG.20335 [PubMed: 17868096]

Pirie A, 1965. A light catalyzed reaction in the aqueous humor of the eye. Nature 205, 500–501. 10.1038/205500A0 [PubMed: 14265299]

Rivera S, Nemeth E, Gabayan V, Lopez MA, Farshidi D, Ganz T, 2005. Synthetic hepcidin causes rapid dose-dependent hypoferremia and is concentrated in ferroportin-containing organs. Blood 106, 2196–2199. 10.1182/BLOOD-2005-04-1766 [PubMed: 15933050]

Rouault TA, Tang CK, Kaptain S, Burgess WH, Haile DJ, Samaniego F, McBride OW, Harford JB, Klausner RD, 1990. Cloning of the cDNA encoding an RNA regulatory protein--the human iron-responsive element-binding protein. Proc. Natl. Acad. Sci. U. S. A 87, 7958–7962. 10.1073/PNAS.87.20.7958 [PubMed: 2172968]

Schindelin J, Arganda-Carreras I, Frise E, Kaynig V, Longair M, Pietzsch T, Preibisch S, Rueden C, Saalfeld S, Schmid B, Tinevez J-Y, White DJ, Hartenstein V, Eliceiri K, Tomancak P, Cardona A, 2012. Fiji: an open-source platform for biological-image analysis. Nat. Methods 2012 97 9, 676–682. 10.1038/nmeth.2019

Schleicher RL, Carroll MD, Ford ES, Lacher DA, 2009. Serum vitamin C and the prevalence of vitamin C deficiency in the United States: 2003–2004 National Health and Nutrition Examination Survey (NHANES). Am. J. Clin. Nutr 90, 1252–1263. 10.3945/AJCN.2008.27016 [PubMed: 19675106]

Shu W, Baumann BH, Song Y, Liu Y, Wu X, Dunaief JL, 2019. Iron Accumulates in Retinal Vascular Endothelial Cells But Has Minimal Retinal Penetration After IP Iron Dextran Injection in Mice. Invest. Ophthalmol. Vis. Sci 60, 4378. 10.1167/IOVS.19-28250 [PubMed: 31634395]

Sterling J, Guttha S, Song Y, Song D, Hadziahmetovic M, Dunaief JL, 2017. Iron importers Zip8 and Zip14 are expressed in retina and regulated by retinal iron levels. Exp. Eye Res 155, 15–23. 10.1016/J.EXER.2016.12.008 [PubMed: 28057442]

Syed BA, Beaumont NJ, Patel A, Naylor CE, Bayele HK, Joannou CL, Rowe PSN, Evans RW, Srai SK, 2002. Analysis of the human hephaestin gene and protein: comparative modelling of the N-terminus ecto-domain based upon ceruloplasmin. Protein Eng 15, 205–214. 10.1093/PROTEIN/15.3.205 [PubMed: 11932491]

Wolkow N, Song D, Song Y, Chu S, Hadziahmetovic M, Lee JC, Iacovelli J, Grieco S, Dunaief JL, 2012. Ferroxidase Hephaestin's Cell-Autonomous Role in the Retinal Pigment Epithelium. Am. J. Pathol 180, 1614. 10.1016/J.AJPATH.2011.12.041 [PubMed: 22342521]

Wolkow N, Song Y, Wu T-D, Qian J, Guerquin-Kern J-L, Dunaief JL, 2011. Aceruloplasminemia: retinal histopathologic manifestations and iron-mediated melanosome degradation. Arch. Ophthalmol. (Chicago, Ill. 1960) 129, 1466–1474. 10.1001/ARCHOPHTHALMOL.2011.309

Zhao J, Kim HJ, Ueda K, Zhang K, Montenegro D, Dunaief JL, Sparrow JR, 2021. A vicious cycle of bisretinoid formation and oxidation relevant to recessive Stargardt disease. J. Biol. Chem 296. 10.1016/J.JBC.2021.100259

Zhao N, Zhang AS, Worthen C, Knutson MD, Enns CA, 2014. An iron-regulated and glycosylation-dependent proteasomal degradation pathway for the plasma membrane metal transporter ZIP14. Proc. Natl. Acad. Sci. U. S. A 111, 9175–9180. 10.1073/PNAS.1405355111/-/DCSUPPLEMENTAL [PubMed: 24927598]

Highlights

1. Neural retina-specific deletion of hephaestin results in neural retina iron accumulation
2. Retinal ganglion cells have elevated transferrin receptor
3. Retinal degeneration does not occur in this mouse line

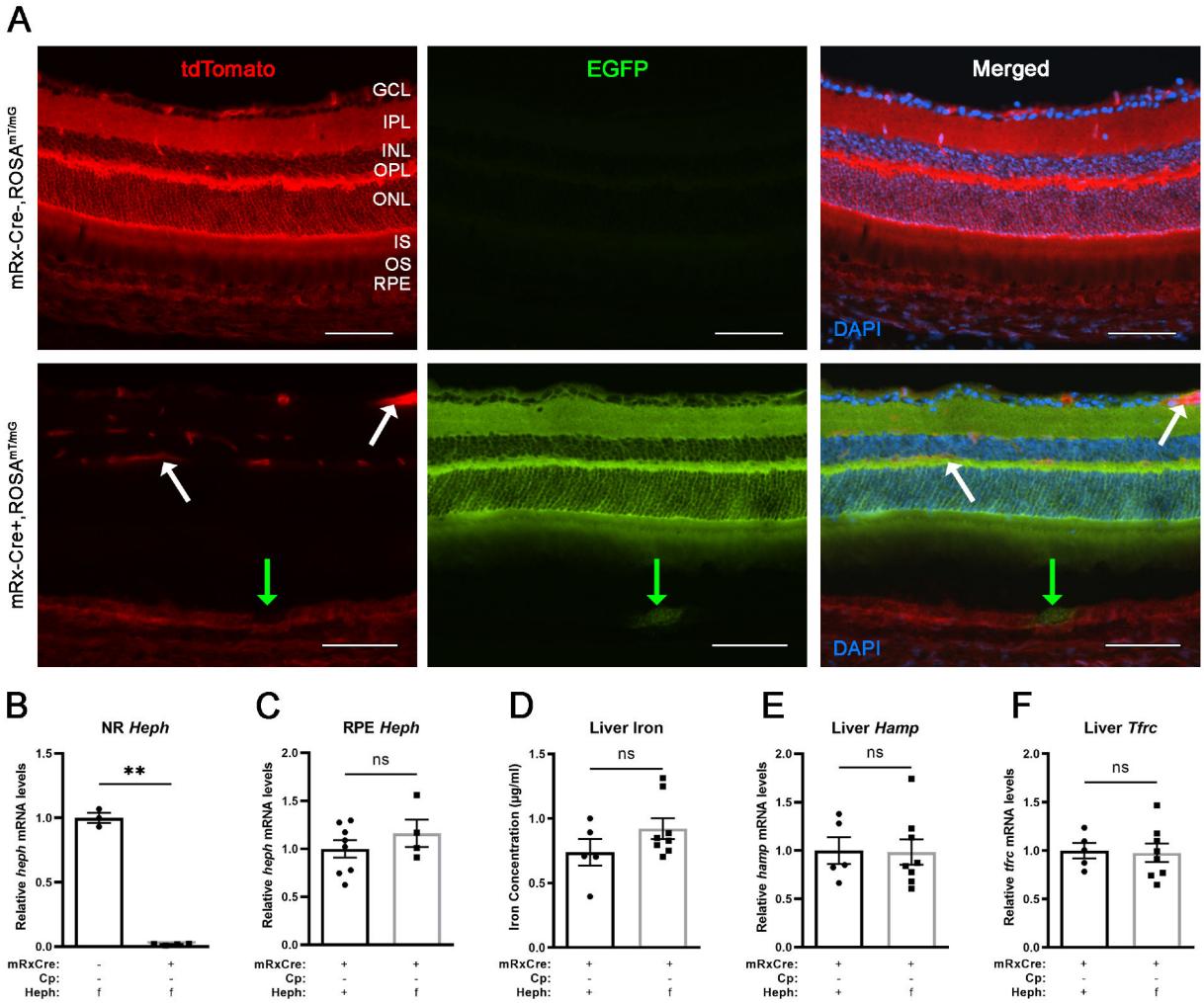

Figure 1. Validation of mRx-Cre experimental mice.

(A) Representative images of native retina fluorescence of the mRx-Cre+, ROSA$^{mT/mG}$ mouse line. White arrows indicate blood vessels and green arrows point to an RPE cell. **(B)** qPCR measurement of neural retina *Heph* mRNA expression. **(C)** qPCR measurement of RPE *Heph* mRNA expression. **(D)** Liver iron concentration measurements by a BPS assay. **(E)** qPCR measurement of liver hepcidin (*Hamp)* mRNA expression. **(F)** qPCR measurement of liver *Tfrc* mRNA expression. Graphs show mean values (±SEM), ** $p < 0.01$. The scale bar is 100 µm.

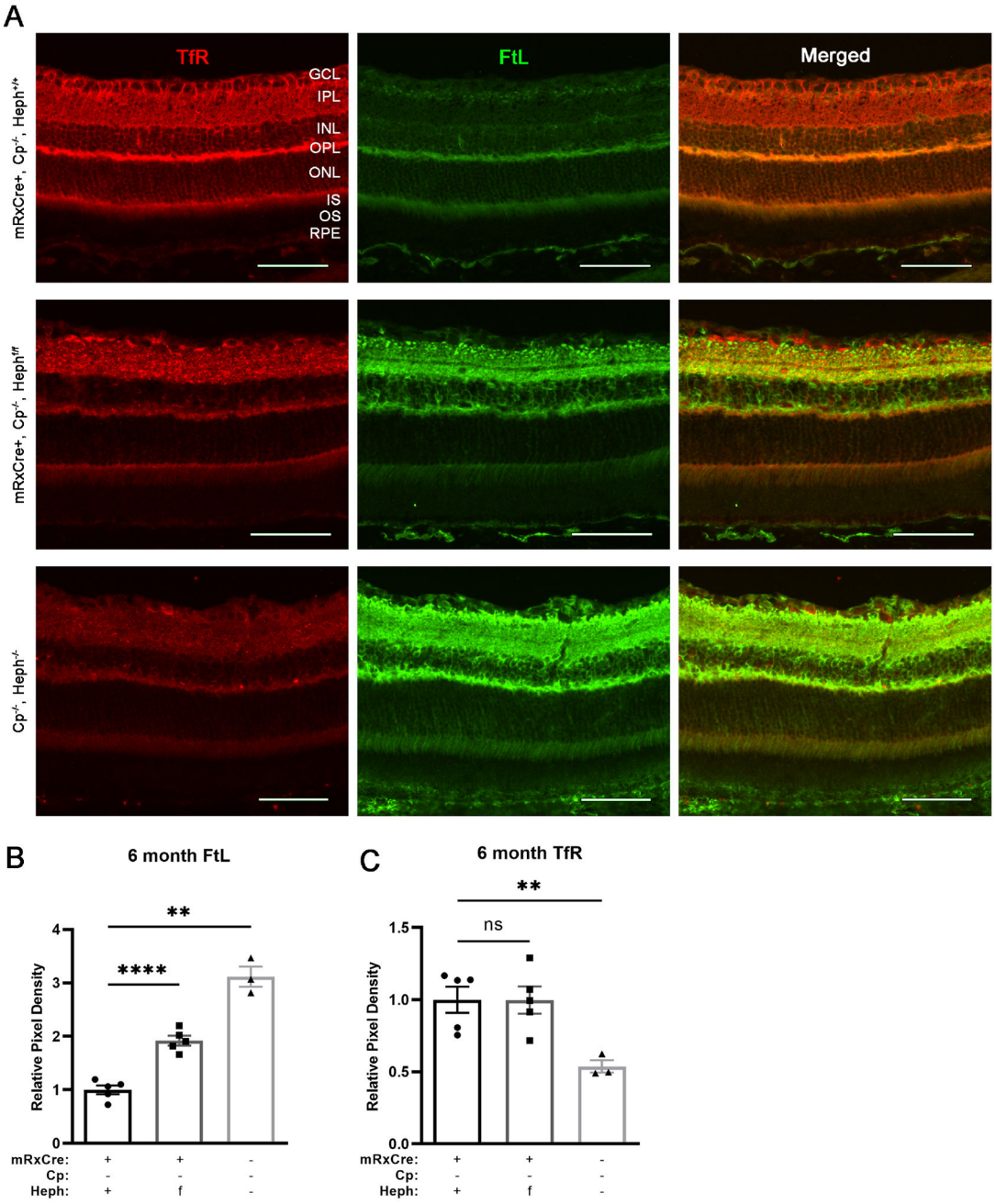

Figure 2. Ferritin-L accumulates in retinas of mRx-Cre+, *Cp*$^{-/-}$, *Heph*$^{flox/flox}$ mice.

(A) Representative immunofluorescence images for TfR (red) and FtL (green) in *mRx-Cre+, Cp*$^{-/-}$*, Heph*$^{flox/flox}$ (experimental), *mRx-Cre+, Cp*$^{-/-}$*, Heph*$^{+/+}$ (control), and systemic *Cp*$^{-/-}$*, Heph*$^{-/-}$ mice at 6 months. **(B)** Pixel density analysis for FtL on 6-month-old mice. **(C)** Pixel density analysis for TfR on 6-month-old mice. Pixel density analysis was performed on two technical replicates per mouse and the results averaged per mouse. Graphs represent mean values ±SEM, ** $p < 0.01$, **** $p < 0.0001$. The scale bar is 100 μm.

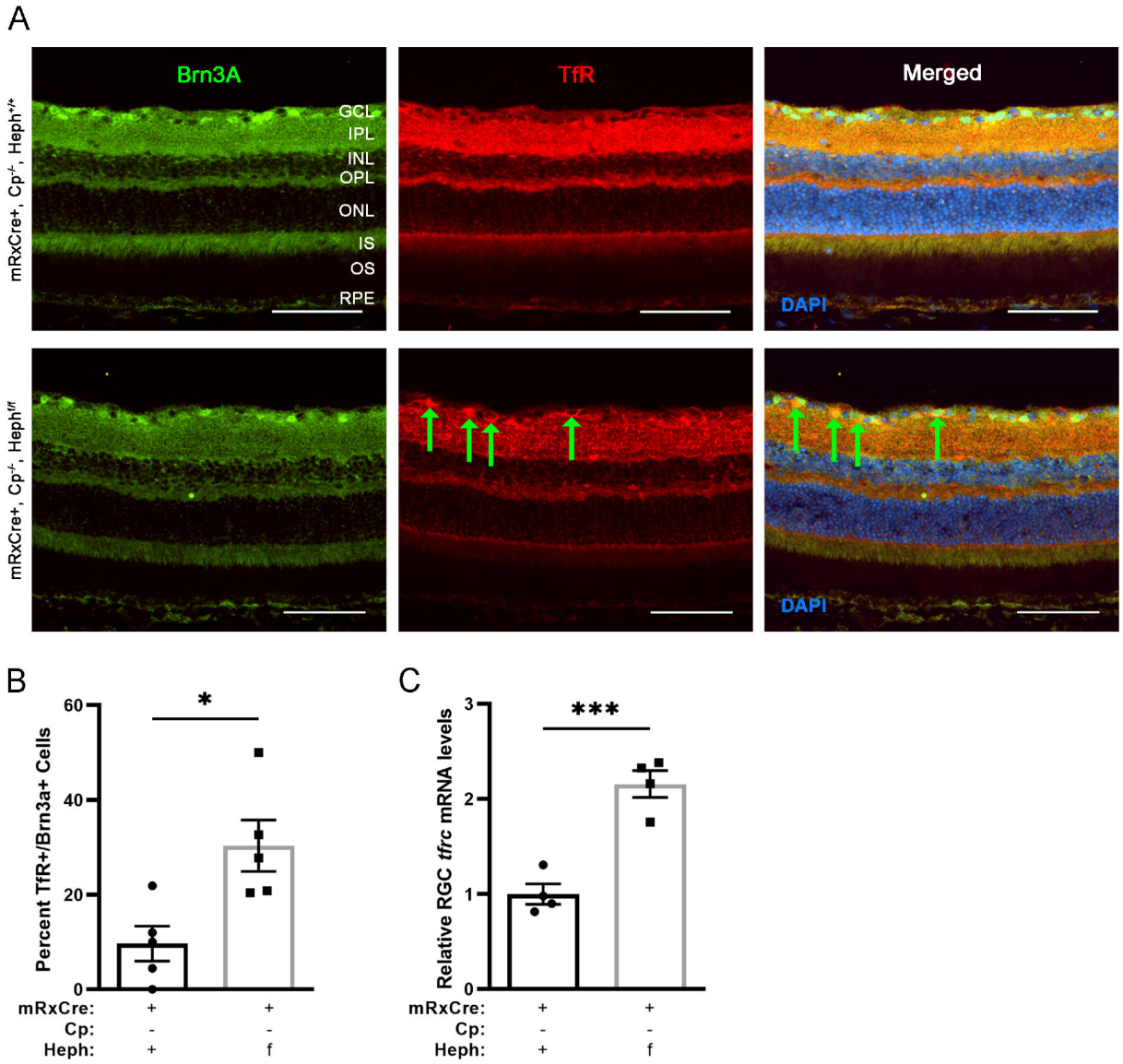

Figure 3. Retinal ganglion cells have elevated TfR in mRx-Cre+, $Cp^{-/-}$, $Heph^{flox/flox}$ mice.

(A) Representative immunofluorescence images of retinas labeled with Brn3a (green) and anti-TfR (red) in 6-month-old mice. Green arrows point to elevated TfR signal in the ganglion cell layer. **(B)** Quantification of cells doubly positive for TfR and Brn3a. **(C)** qPCR measurement of *Tfrc* mRNA expression in isolated RGCs. Graphs represent mean values ±SEM, * $p < 0.05$, *** $p < 0.001$. The scale bar is 100 μm.

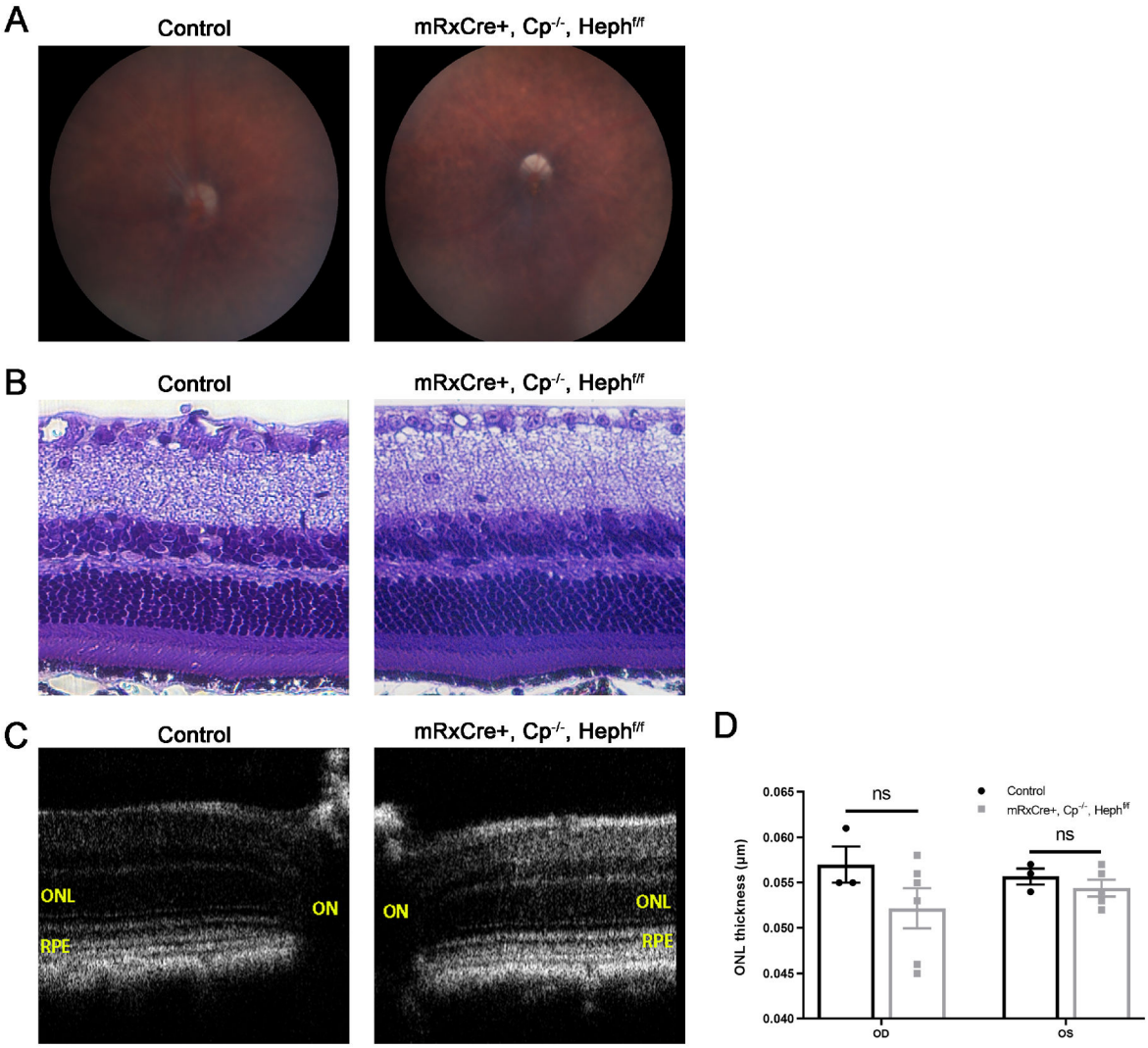

Figure 4. mRx-Cre+, $Cp^{-/-}$, $Heph^{flox/flox}$ mice do not have altered retinal morphology at age 12 months.

(A) Micron III *in vivo* retina photographs. **(B)** Representative images of toluidine blue stained plastic sections. **(C)** Representative OCT images. **(D)** Outer nuclear layer thickness measurements. Control mice had genotypes mRx-Cre+, $Cp^{-/-}$, $Heph^{+/+}$ (n=1) or mRx-Cre+, $Cp^{+/-}$, $Heph^{flox/flox}$ (n=2). Graphs represent mean values ±SEM.